LIGHT AND FREQUENCY ANALYSIS OF DETACHED ECCENTRIC BINARY SYSTEM DT CAM WITH PRE-MAIN SEQUENCE COMPONENT

Tuncay ÖZDEMİR[1] and Birol GÜROL[2]

Draft version: March 4, 2024

RESUMEN

ABSTRACT

In this study we analyzed *TESS* data of detached eccentric binary system DT Cam and the first physical parameters of the components were obtained. We found that out of eclipse variation of the system shows a small amplitude periodic variation. Most of the frequencies obtained are related with the orbital variation except one which the period was determined as ~ 0.605 days. The masses and radii of the primary and secondary components were calculated as $M_1 = 1.793 M_\odot$, $M_2 = 1.414 M_\odot$, $R_1 = 1.355 R_\odot$, and $R_2 = 1.522 R_\odot$, respectively. Considering the physical properties of the primary component we conclude that it is a rotational variable. We found that the massive component is smaller than the low-mass component. It seems that the secondary component is a pre-main sequence star which is very important for understanding of stellar structure and evolution.

Key Words: binaries: eclipsing — individual: (DT Cam) — techniques: photometric — Stars: fundamental parameters — Stars:variable:rotation

1. INTRODUCTION

DT Cam (TIC 87251422, HD 33500, $\alpha_{2000} = 05^h 13^m 57^s.69$, $\delta_{2000} = +56° 30' 28''.61$, $V = 8^m.13$) is classified as a Spectroscopic Binary in the Simbad[3] database. The spectral type and distance of the system were given as A2 (Cannon and Pickering 1993) and 184 pc (*Gaia* Collaboration 2022), respectively. The system was defined as an Algol-type eclipsing binary by Otero et al. (2005) with orbital period of P=14.132500 days, and it is included in the GCVS catalogue[4].

In the catalogue of published by McDonald et al. (2012), the system's distance (d), effective temperature ($T_{\rm eff}$), and luminosity (L) given as d=255.750 pc, $T_{\rm eff} = 7948$ K, and $L = 27.52 L_\odot$, respectively. In the Eclipsing Binary Catalogue published by Avvakumova et al. (2013) the system is classified as DM (Detached Main Sequence System) with depth of the primary minima as

---

[1]Department of Physics, Faculty of Arts and Sciences, İnönü University, Malatya, TURKEY.

[2]Department of Astronomy and Space Sciences, Ankara University Science Faculty, Tandoğan, Ankara, TURKEY.

[3]https://simbad.cds.unistra.fr/simbad/

[4]http://www.sai.msu.su/gcvs/cgi-bin/search.html

$0^m.06$ which is probably mistyped. By analyzing the eclipse timing diagram of the system, Kim et al. (2018) found the orbital period and the phase of the secondary minima as P=7.0662668 days and 0.578, respectively. Zasche et al. (2018) do the first light curve and $(O-C)$ analysis of the system by using unfiltered and special SuperWASP observations and obtained the system parameters as given in Table 1.

TABLE 1

PARAMETERS OF THE LIGHT CURVE AND THE $(O-C)$ ANALYSES OF DT CAM OBTAINED BY ZASCHE ET AL.(2018).

Parameter	Value
i(deg)	87.69 (0.19)
T_1(K)	8800
T_2(K)	7382 (75)
L_1(%)	66.4 (0.7)
L_2(%)	33.6 (0.6)
L_3(%)	0.0
R_1/a	0.068(3)
R_2/a	0.064(2)
e	0.188(0.010)
$\omega(deg)$	49.2(1.3)
U(yr)	>100

By using Gaia DR2 data, Kervella et al. (2019) obtained color excess, system's radial velocity, mass and radius of the primary component as $E(B-V) = 0.087$, $V_R = 33.881\,\mathrm{km/s}$, $M_1 = 2.2 M_\odot$ and $R_1 = 1.862 R_\odot$, respectively. Later by using Gaia EDR3 data, Kervella et al. (2022) updated some of the parameters as $V_R = 33.76\,\mathrm{km/s}$, $M_1 = 2.20 M_\odot$ and $R_1 = 1.85 R_\odot$. In the catalogue of EA-type eclipsing binaries observed by *TESS* data published by Shi et al. (2022) the system's orbital period was given as 14.1325 days. Based on the Multi-site All-Sky CAmeRA (MASCARA) observations (see Fig.1) published by Burggraaff et al. (2018) the depth of the primary and secondary minima were given as $0^m.75$ and $0^m.2$, respectively. In Fig.1 although scattering observed at the maxima light, there are also traces of periodic variation which can be related to pulsation in the system.

2. THE *TESS* DATA AND LIGHT ELEMENTS

The observations of DT Cam were made by the Transiting Exoplanet Survey Satellite (*TESS*) (Ricker et al. 2015) in Sectors 19 and 59 with each sector having ~27.4 days of observations with nearly 2 min (SC: Short Cadence) exposure time. The *TESS* data are public in the MAST (Barbara A. Mikulski Archive for Space Telescopes[5]) archive. In this study we prefer to use the raw

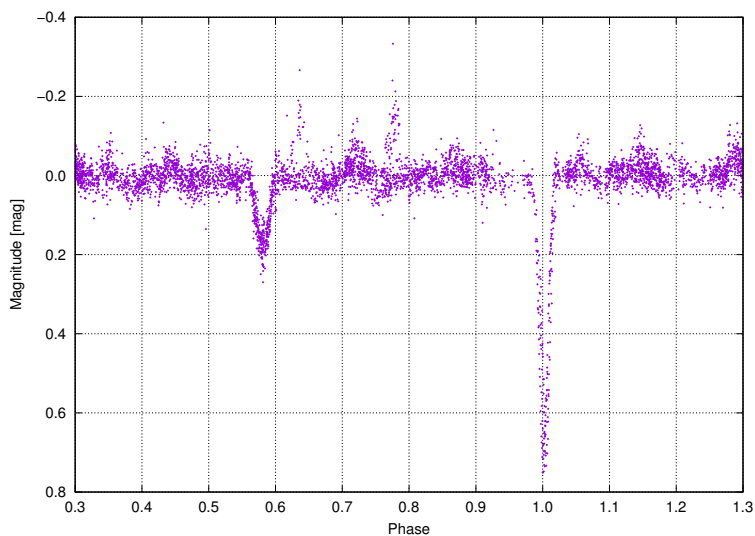[5]https://mast.stsci.edu/portal/Mashup/Clients/Mast/Portal.html

Fig. 1. Unfiltered light curve of ASCC 178636 (DT Cam) observed from MASCARA published by Burggraaff et al. (2018).

SAP (simple aperture photometry) data. A total of 35,860 observations of the system were obtained and the time span is nearly 1120.6 days. The light elements of the system are given in the *TESS* Eclipsing Binary Catalogue[6] published by Prša et al. (2022) as,

$$Min.I(BJD) = 2458825.166288(0.000014) + 7.0661708(0.000206) \times E \quad (1)$$

In Fig.2 we plotted the light curve of the system obtained in Sectors 19 and 59 by using the light elements given by Prša et al. (2022). As can be seen in the zoomed inner plot of the secondary minima for both sectors does not overlap with each other which indicates that the light elements of the system need to be refined. Same situation is occurred in primary minima too but does not shown here. Additionally from the light curve we can say that the eclipsing system composed of two spherical components in detached (D) configuration, and because of the secondary minima occurred out of 0.5 phases including the duration of the eclipse times are different with each other we can say that the eccentricity of the system must be larger than zero.

Since the light elements given with Eq.(1) by Prša et al. (2022) was derived from using only sector 19 data, we primarily obtained a full set of minima times from current observations. Using the *TESS* observations, we obtained 8 primary and 7 secondary eclipse times. The eclipse times were calculated by using the Minima27[7] software published by Dr. Bob Nelson. In Table
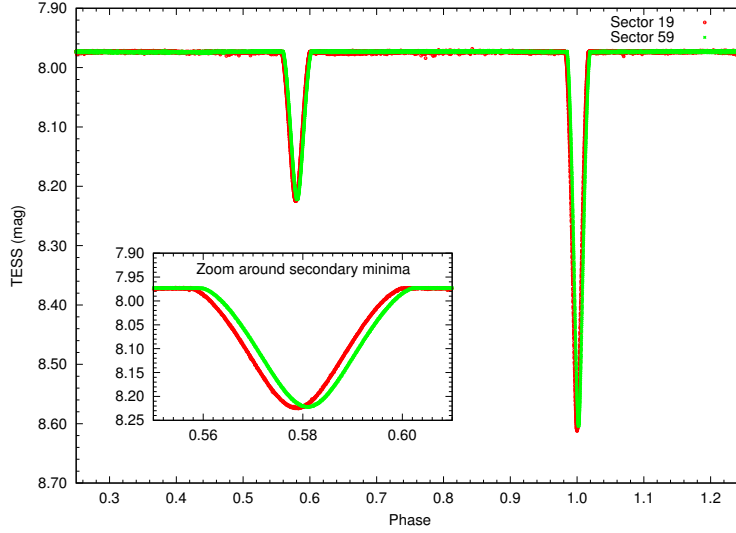

Fig. 2. The plotted light curve of DT Cam (TIC 87251422) obtained from MAST archive for Sectors 19 (red) and 59 (green). The orbital phase calculated by using Eq.(1).

2, we present the calculated minima times with their errors. Additionally, we included the minima times found in the literature. The minima times published in HJD converted to BJD using the algorithm published by Eastman et al. (2010)[8].

The time span of the primary and secondary minima is about 11,433 and 3639 days, respectively. Applying a linear fit on the $(O - C)$ data (see Fig.3) we obtained new light elements as,

$$Min.I(BJD) = 2458825.167737(0.00109) + 7.06625839(0.00000202) \times E \quad (2)$$

$$Min.II(BJD) = 2458822.747588(0.00214) + 7.06622709(0.00001452) \times E \quad (3)$$

The difference in orbital periods calculated for the primary and secondary minima is about 1.079 sec which is smaller than the obtained errors. Probably this difference occurred because of the different time span of the times of minima used in the fit. The ratio of the slopes obtained for the fit is ~0.875. Because of this, the $(O-C)$ values between the primary and secondary minima is going to be larger at bigger Epoch values. We think that there is not enough data or time span to draw a firm conclusion about apsidal motion as mentioned by Zasche et al. (2018). For the rest of the calculation, we used the light elements obtained for the primary minima.

---

[8]https://astroutils.astronomy.osu.edu/time/hjd2bjd.html

TABLE 2

THE OBTAINED ECLIPSE TIMES AND ERRORS OF THE DT CAM.

| No	Min.Type	HJD (2400000+)	BJD (2400000+)	$\pm\sigma$	References
1	I	48501.35500	48501.35568	-	Otero et al. (2005)
2	I	48543.75800	48543.75868	0.03	Kim et al. (2018)
3	I	51476.27300	51476.27373	0.02	Kim et al. (2018)
4	I	55977.46852	55977.46928	0.00011	Zasche et al. (2014)
5	I	55984.52776	55984.52852	0.00292	Zasche et al. (2018)
6	I	56203.58753	56203.58830	0.00016	Zasche et al. (2014)
7	I	56281.31626	56281.31703	0.00019	Zasche et al. (2017)
8	II	56292.47172	56292.47249	0.00058	Zasche et al. (2017)
9	I	57263.52491	57263.52570	0.0001	Juryšek et al. (2017)
10	I	57355.38700	57355.38780	0.01	Paschke (2017)
11	II	57691.58808	57691.58889	0.00066	Zasche et al. (2017)
12	I	57842.95506	57842.95588	0.00302	Zasche et al. (2018)
13	II	57847.03660	57847.03742	0.0103	Zasche et al. (2018)
14	II	58080.22056	58080.22139	0.0063	Zasche et al. (2018)
15	I	58535.44700	58535.44784	0.0020	Paschke (2019)
16	I	58832.23170	58832.23253	-	Jeong et al. (2020)
17	I	-	58818.10004	0.00001	*TESS*
18	II	-	58822.19000	0.00003	*TESS*
19	I	-	58825.16628	0.00001	*TESS*
20	II	-	58829.25608	0.00003	*TESS*
21	I	-	58832.23254	0.00001	*TESS*
22	II	-	58836.32227	0.00004	*TESS*
23	I	-	58839.29886	0.00001	*TESS*
24	I	59164.34600	59164.34683	0.005	Paschke (2021)
25	II	59182.59000	59182.59083	0.010	Paschke (2021)
26	II	-	59910.39548	0.00002	*TESS*
27	I	-	59913.37222	0.00001	*TESS*
28	II	-	59917.46170	0.00002	*TESS*
29	I	-	59920.43845	0.00001	*TESS*
30	II	-	59924.52798	0.00002	*TESS*
31	I	-	59927.50474	0.00001	*TESS*
32	II	-	59931.59433	0.00002	*TESS*
33	I	-	59934.57104	0.00001	*TESS*
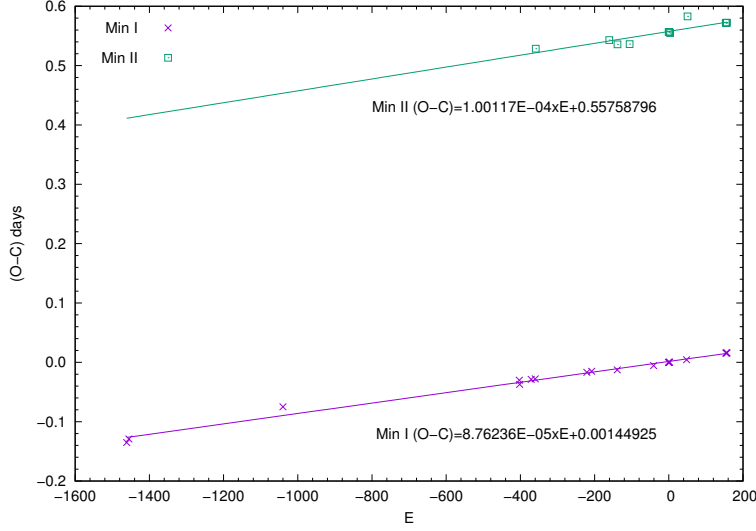
Fig. 3. $(O-C)$ variation and linear fit obtained for DT Cam system by using Eq.(1) published by Prša et al. (2022).

3. LIGHT CURVE ANALYSIS

Because of the calculation time we obtained a total of 1000 points by averaging at 0.001 phase intervals. By using this phase intervals, we see that the depth of both minima was not changed. For the light curve analysis, we prefer to use the Wilson-Devinney (2015 version which in 2019 the *TESS* band added to the code) code which can solve light curves in magnitudes or in flux. The subscripts 1 and 2 refer to the primary (hotter) and the secondary (cooler) component, respectively.

Before light curve analysis we can find eccentricity and argument of periastron of the orbit by using the widths of the primary (w_1) and secondary (w_2) eclipses and the phase of the secondary eclipse (φ_2).

$$e_0 cos w_0 = \frac{\pi}{2}\left[(\varphi_2 - \varphi_1) - 0.5\right] = 0.1241 \tag{4}$$

$$e_0 sin w_0 = \frac{w_2 - w_1}{w_2 + w_1} = 0.1136 \tag{5}$$

The required data given as 0.039, 0.049, and 0.579, respectively by Prša et al. (2022). Using the formulae given by Kopal (1978) (Eq. 4 and 5) and the phase of the primary eclipse as $\varphi_1 = 0$ we obtained the eccentricity and argument of periastron as 0.1683 and 42.48 deg, respectively. And it is used as input parameters in the light curve analysis of the eclipsing system.

In Table 3 we compiled effective temperatures published in different sources except the last one which is obtained according to the $logT_{eff} - (B - V)_0$ relation given by Eker et al. (2020) with using the $(B - V) = 0.20$ color and $E(B - V) = 0.087$ reddening values given by Kervella et al. (2019). The

TABLE 3

T_{EFF} VALUES OBTAINED FROM LITERATURE FOR DT CAM.

T_{eff} (K)	References
8970	Wright et al. (2003)
8589	Ammons et al. (2006)
7948	McDonald et al. (2012)
7947	Chandler et al. (2016)
7962	McDonald et al. (2017)
8006	Tonry et al. (2018)
8006	*Gaia* Collaboration (2018)
8200	Stassun et al. (2019)
7987	Bai et al. (2019)
8200	Paegert et al. (2021)
8381	Eker et al. (2020)

median and average of the effective temperatures are found to be $8006 \pm 329\,\mathrm{K}$ and $8200 \pm 329\,\mathrm{K}$, respectively and we prefer to use these values for the primary component in the light curve analysis of DT Cam.

In the catalogue of Gaia DR3 Part 3 for non-single stars (*Gaia* Collaboration 2022) we found the systems velocity of center of mass as $V_\gamma = 13.111 \pm 0.170\,\mathrm{km/s}$, semi-amplitude of the primary and secondary component as $K_1 = 73.246 \pm 0.406\,\mathrm{km/s}$ and $K_2 = 92.856 \pm 0.400\,\mathrm{km/s}$, respectively. Additionally, the system's eccentricity $e = 0.160 \pm 0.003$ and the argument of periastron $\omega = 39.123 \pm 1.285$ deg were obtained which are compatible with the calculated data by using Eq. (4) and (5). According to the given values in Gaia DR3 catalogue the mass ratio of the system is obtained as $q(m_2/m_1) = 0.7888$.

The Wilson & Devinney method (Wilson & Devinney 1971; Wilson 1979, 1990) was applied to solve the light curve of the DT Cam. In the light curve analysis of the DT Cam, we used Mode 2 for appropriate detached type systems. Additionally, we select the starting parameters as $T_{\mathrm{eff},1} = 8006\,\mathrm{K}$ (Solution 1) and $8200\,\mathrm{K}$ (Solution 2), $e = 0.168$, $\omega = 42.48$ deg, $P = 7.06626244$ days. Because $T_{\mathrm{eff},1}$ is higher than $7200\,\mathrm{K}$, we used the primaries albedo and gravity darkening parameters as 1.0. And assuming the secondary temperature is lower than the primary's we select $T_{\mathrm{eff},2} = 6500\,\mathrm{K}$ including albedo and gravity darkening parameters as 0.5 and 0.32, respectively.

By using the initial parameters (T_1, q, i, e, ω) as input values we solved the light curves until the solution converged. After a coarse solution obtained, we let the l_3 (third-light) parameter free because of the system is located in a crowded region. The convergent solution was obtained with the adjustable parameters by iteration, until the correction on the parameters became smaller than the corresponding standard deviations. The observed and theoretical

light curves, calculated with the final elements, are shown in Fig.4 including
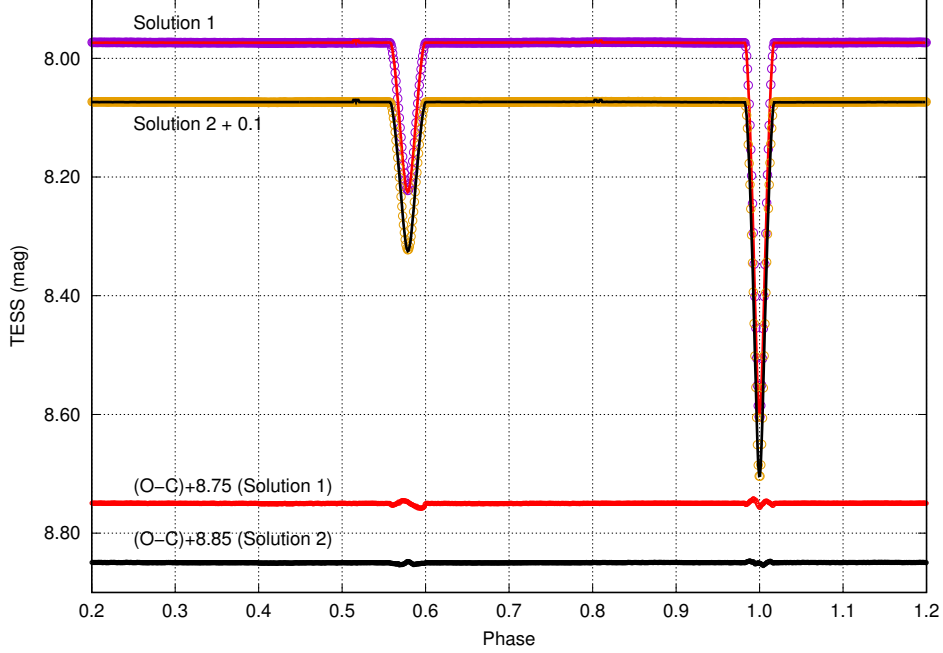the residuals of the fit with the observations.

Fig. 4. The observational and theoretical light curves of DT Cam including the
residuals of the fit for both solution.

The parameters obtained from the light curve analysis are given in Table 4.
The absolute parameters of the components obtained by the Wilson-Devinney
LC code for the DT Cam system are given in Table 5. Because the LC code
does not give the errors of the absolute parameters, we estimated them from
the input parameters. The errors given here correspond to the propagated
errors of the calculated parameters.

Using the bolometric magnitude and bolometric correction for the primary
component as 2.694 ± 0.178 and 0.022, respectively, we obtained the absolute
magnitude of the primary component as $M_{V,1} = 2.672 \pm 0.279$. In the ASAS-
SN Catalogue of Variable Stars II database[9] the mean V magnitude of the
system was given as $8^m.63$ and it is nearly 0.5 magnitude dimmer than the
given value in the Simbad database. The $(B-V)$ and $E(B-V)$ values given in
the ASAS-SN Catalogue as 0.093 and 0.577, respectively, are different than the
values found in the literature. By using $(B-V) = 0.2$ and $E(B-V) = 0.07$ we

_____

[9]https://asas-sn.osu.edu/variables/531066b2-10c7-52cb-8856-d6a54c9843ee

TABLE 4

THE LIGHT CURVE SOLUTION OF DT CAM.

Parameters	Solution 1		Solution 2	
	Value	$\pm\sigma$	Value	$\pm\sigma$
T_0(BJD)	2458825.16774	0.00109	-	-
P (day)	7.06625839	0.000002	-	-
a($R_\odot$)	22.859	0.024	-	-
V_γ(km/s)	13.111	0.170	-	-
K_1(km/s)	73.246	0.406	-	-
K_2(km/s)	92.856	0.400	-	-
e	0.167	0.001	0.164	0.002
ω(deg)	42.643	0.029	41.060	0.059
$q(m_2/m_1)$	0.7888	-	-	-
Phase Shift	0.0360	-	0.0360	-
i(deg)	87.675	0.006	88.194	0.010
T_1(K)	8006*	329*	8200*	329*
T_2(K)	6368	250*	6448	250*
A_1	1.000	-	1.000	-
A_2	0.500	-	0.500	-
g_1	1.000	-	1.000	-
g_2	0.320	-	0.320	-
Ω_1	17.82053	0.00665	18.10684	0.01549
Ω_2	13.15815	0.00381	13.08262	0.00824
x_1 (bolo)	0.651	-	-	-
x_2 (bolo)	0.640	-	-	-
y_1 (bolo)	0.255	-	-	-
y_2 (bolo)	0.234	-	-	-
$L_1/L_{tot}(TESS)$	0.60057	0.00078	0.59815	0.00148
$L_3/L_{tot}(TESS)$	0.00920	-	0.01639	-
r1(mean)	0.05928	0.00002	0.05827	0.00003
r2(mean)	0.06658	0.00002	0.06697	0.00003
σ(fit)	-	2.6245E-07	-	5.3357E-07

Assumed values marked with asterisks.

obtained the interstellar extinction in V filter as $A_v = 3.1 \times E(B-V) = 0.317$. Using those values, we obtained the distance of the DT Cam as 174 ± 10 pc which is consistent with that given in the *TESS* Input Catalogue (Stassun et al. 2019) and Gaia DR3 catalogues as 183.927 and 183.479 pc, respectively.

4. OUT OF ECLIPSE LIGHT VARIATION

Due to the relatively large amplitude of the eclipse variation, we cannot visually see any light variations at the maxima of the light curve. In Fig.4, we see that the light at the maxima is fairly smooth. Since the primary component's temperature is located in the instability strip, we suspected that it could be a pulsator, similar to δ Scuti or γ Dor stars. In Fig.5 we plot the out-of-eclipse variation for Sectors 19 (upper panel) and 59 (lower panel) included

TABLE 5

ABSOLUTE PARAMETERS OF DT CAM.

Parameters	Solution 1		Solution 2	
	Primary	Secondary	Primary	Secondary
Mass ($M_\odot$)	1.793 ± 0.007	1.414 ± 0.006	1.793 ± 0.007	1.414 ± 0.006
Radius ($R_\odot$)	1.340 ± 0.002	1.538 ± 0.002	1.332 ± 0.002	1.531 ± 0.002
Luminosity* ($L_\odot$)	6.796 ± 1.117	3.432 ± 0.539	7.227 ± 1.160	3.651 ± 0.566
$\rho(\rho_\odot)$	0.721	0.401	0.759	0.394
M_{bol}	2.669 ± 0.178	3.411 ± 0.171	2.603 ± 0.174	3.344 ± 0.168
Bol.Corr.(BC)	0.022	0.062	0.003	0.068
M_v	2.647 ± 0.279	3.349 ± 0.274	2.600 ± 0.277	3.276 ± 0.273
log g (cgs)	4.428 ± 0.002	4.224 ± 0.002	4.443 ± 0.002	4.219 ± 0.002
d(pc)	174 ± 10	-	178 ± 10	-

* Calculated by using components' temperature and radius.

the eclipse boundaries with the regions of ingress and egress to the eclipse indicated with horizontal error bars. As can be seen in Fig.5 despite scattering (gray dots) there are multi periodic variation which can be attributed to a pulsation or any other type of variation like rotation in the system. Because of scattering, we prefer to smooth the light curves by obtaining an average of 5 successive observations (black dots in Fig.5).
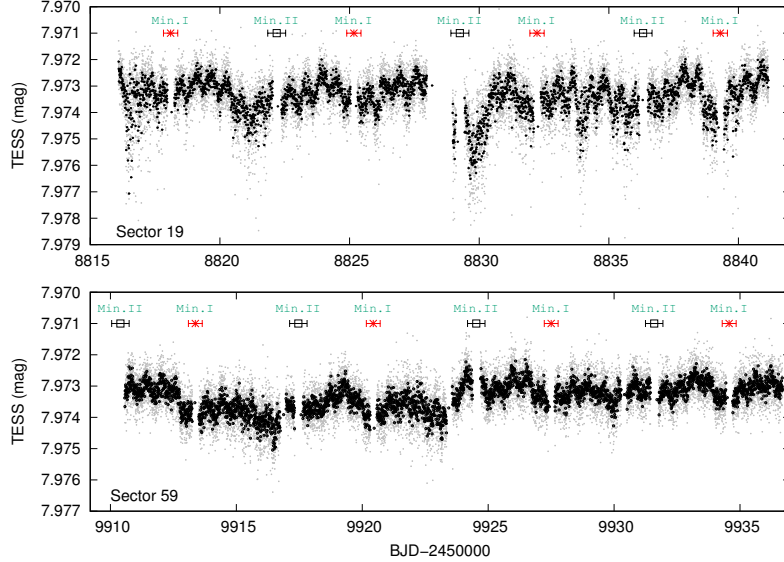

Fig. 5. Out-of-eclipse variation of DT Cam for Sectors 19 (upper panel) and 59 (lower panel). Black dots represent the average of 5 successive observations.

The time gap between Sector 19 and 59 is approximately 1069 days. Because of this we prefer to analyze the data separately in the frequency domain. The obtained frequencies were given in Table 6, and the amplitude variation in Fig.6 includes the Fourier fit in Fig.7. The Rayleigh resolution for the Sectors

TABLE 6

THE OBTAINED SIGNIFICANT FREQUENCIES OF DT CAM USING
OUT-OF-ECLIPSE DATA FOR SECTORS 19 AND 59.

No	Frequency (d^{-1})	Amplitude *TESS* (mag)	Phase (rad)	P(days)	P_{orb}/P	n	Difference	Combination
				Sector 19				
f_1	1.650234	0.000324	0.119240	0.60597	11.661	-	-	-
f_2	0.227481	0.000198	0.613891	4.39598	1.607	-	-	-
f_3	0.431016	0.000162	0.622711	2.32010	3.046	3	-0.0065	$3f_{orb}$
f_4	0.277367	0.000325	0.363430	3.60533	1.960	2	0.0057	$2f_{orb}$
f_5	0.133695	0.000213	0.403955	7.47972	0.945	1	0.0078	f_{orb}
f_6	0.319271	0.000168	0.512517	3.13213	2.256	-	-	-
f_7	0.041904	0.000141	0.513211	23.86387	0.296	-	-	-
				Sector 59				
f_1	0.034459	0.000330	0.634004	29.02023	0.243	0.25	0.0009	$f_{orb}/4$
f_2	1.652104	0.000180	0.165151	0.60529	11.674	-	-	-
f_3	0.141664	0.000170	0.828329	7.05898	1.001	1	-0.0001	f_{orb}
f_4	0.428820	0.000206	0.133727	2.33198	3.030	3	-0.0043	$3f_{orb}$
f_5	0.070832	0.000153	0.887096	14.11795	0.501	0.5	-0.0001	$f_{orb}/2$
f_6	0.277584	0.000103	0.481096	3.60251	1.961	2	0.0055	$2f_{orb}$
f_7	0.111034	0.000097	0.965751	9.00628	0.785	-	0.0038	$f_3 - f_1$ (f_{orb}-$f_{orb}/4$)

19 and 59 were obtained as $0.040d^{-1}$ and $0.038d^{-1}$, respectively. All of the marked combinations given in Table 6 are obtained as the difference between the observed and the predicted frequencies which are smaller or equal to the Rayleigh criterion.

The existence of periodic variation can be clearly seen by using the normal points created. We found that most of the frequencies obtained are related with the orbital period except the frequency obtained at $1.65d^{-1}$ which corresponds to 0.605 days. The strongest amplitude (essentially semi-amplitude) is in the order of 0.0003 mag in *TESS* filter. The amplitude in Johnson V is not known but we can estimate it using the relation given by Paunzen et al. (2020) as $Amp(V)/Amp(TESS) = 1.44(4)$. According to this relation, the estimated amplitude in Johnson V is about 0.00086 mag and we cannot obtain such a low magnitude variation with ordinary photometric Earth observations. As can be seen in Fig.6, the real amplitude of the periodic variation is probably larger than obtained by Fourier analysis.

Grigahcène et al. (2010) characterized the δ Scuti type variables as short period pulsating stars, with periods between 0.014 (f = 71.428 d^{-1}) and 0.333 (f = 3.003 d^{-1}) days with pulsation constant Q (Handler et al. 2002) lower than 0.055 days, and generally the accepted lower limit is smaller than 0.033 days (Stellingwerf 1979; Breger 1990).

The binary model yields a mean density of $\rho_1 = 0.721\rho_\odot$ and $\rho_2 = 0.401\rho_\odot$ for primary and secondary component, respectively. The frequency for the highest amplitude variations for Sector 19 found to be $f_1 = 1.650234d^{-1}$ ($P_1 = 0.60597$ days). Using the relation given as $Q = P_{puls}\sqrt{(\rho/\rho_\odot)}$, we obtained pulsation constant as $Q_1 = 0.514$ and $Q_2 = 0.384$ days for the primary and secondary component, respectively. As can be seen all of the pulsation constants are larger than 0.055 days. According to these results,
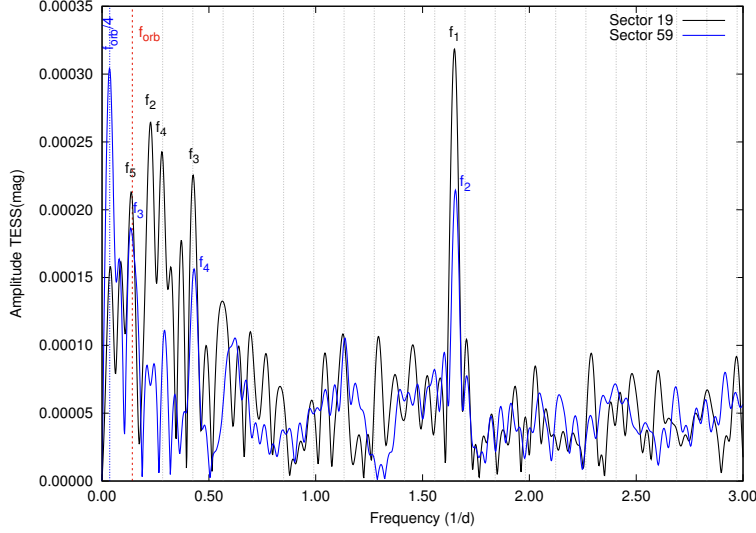
Fig. 6. The amplitude spectrum for the out-of-eclipse light variation of DT Cam for Sectors 19 (black line) and 59 (blue line). We marked the location of the orbital frequency (red vertical line) including the harmonics of orbital frequency f_{orb} with gray vertical lines.

including the period of the cyclic variation we conclude that no one of the components can be an δ Scuti pulsator.

The location of secondary component in the HR diagram coincides with the Solar-like pulsators but the pulsation period is much larger than the 3 to 10 min ranges as given by Aerts et al. (2010). Because of this we conclude that the secondary component cannot be a Solar-like pulsators.

Kaye et al. (1999) characterized the γ Doradus (GDOR) type variables as high-order, low-degree, non-radial gravity mode pulsators and showed that the period range is $0.3 \leq P(day) \leq 3(0.33 \leq f(d^{-1}) \leq 3.33)$. Among the GDOR type pulsators there are low- and high-amplitude examples which the high-amplitude ones explained by the superposition of several base frequencies (Paunzen et al. 2020). Most of the GDOR pulsators are in the region of A- and F-type main sequence stars which the temperature range of $6100 < T_{\rm eff} < 7500\,$K (Bradley et al. 2015). Additionally, Q pulsation constants for GDOR type stars is given as $Q > 0.24$ days (Grigahcène et al. 2010).

All of the parameters obtained for the secondary component; effective temperature ($T_2 = 6368\,$K), Q pulsation constant ($Q_2 = 0.384$ days), and frequency of the periodic variation ($f = 1.65d^{-1}$) shows us that the secondary component can be a GDOR type pulsator. In Fig.8 we see that the secondary component is located out of the instability strip given for GDOR type pulsators. But we also see that a small number of GDORs are located outside this instability strip too which can be a sign of confirmation of the type of the pulsator.

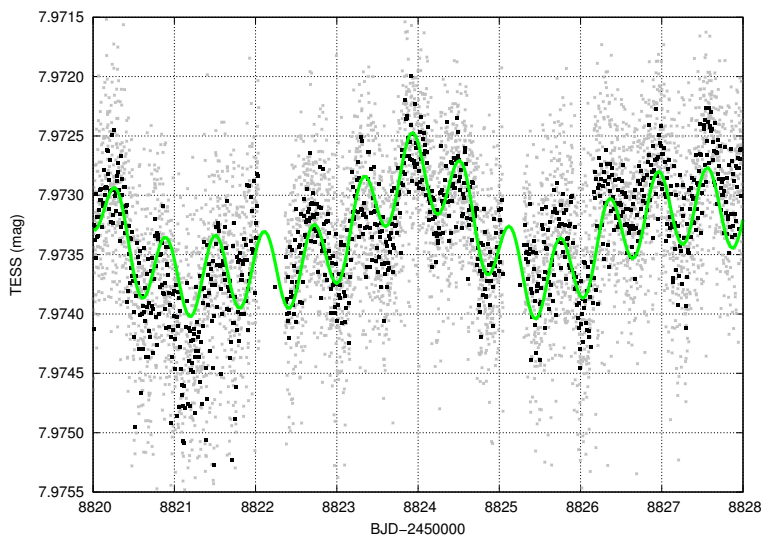By using Kepler observations, Balona (2011) showed that low-frequency

Fig. 7. Small amplitude periodic variation of DT Cam at Sector 19 (a small portion was plotted). The synthetic curve was computed using all the frequencies detected. Gray dots are for the original data, black dots represent the average of 5 successive observations, and green line is the Fourier fit obtained by using all of the frequencies given in Table 6 for Sector 19.

variations are present in most A-type stars and that the dominant period is consistent with the expected rotational periods of these stars. Using this finding Balona (2011) suggest that starspots, or other corotating structures, may be responsible for the low-amplitude light variations in normal A-type stars. Comparison of the two sectors with each other in Fig. 6 (the amplitude of frequency at 1.65 d^{-1}) we see that the amplitude is essentially different in both sectors which can be a sign to variable amplitude. And this can be a sign of starspots as mentioned by Lanza et al. (2009) for cool stars. Because of this there is a possibility of the secondary component having starspots on the surface, which is the cooler component of the eclipsing system. Balona (2011) showed that there is a possibility of the A-type component also having starspots on surface, and found that a total of 208 A-type stars which is coded as SPOT in their work shows only a single peak in the frequency domain as we obtained for the DT Cam system

Assuming that the frequency of highest amplitude is the rotation frequency we can calculate the rotational velocity of the components separately by using radius values given in Table 5. The rotational velocities obtained for primary and secondary components are $v_1 = 112.57$ km/s and $v_2 = 129.20$ km/s, respectively. In the literature we found that the average rotational velocities of A0 and F5 type main-sequence stars were given as 190 and 25 km/s, respectively (McNally 1965). Using the corresponding spectral types for the components as A2+F4 we concluded that the low amplitude periodic variation with period of 0.60597 days can be caused by the rotation of primary
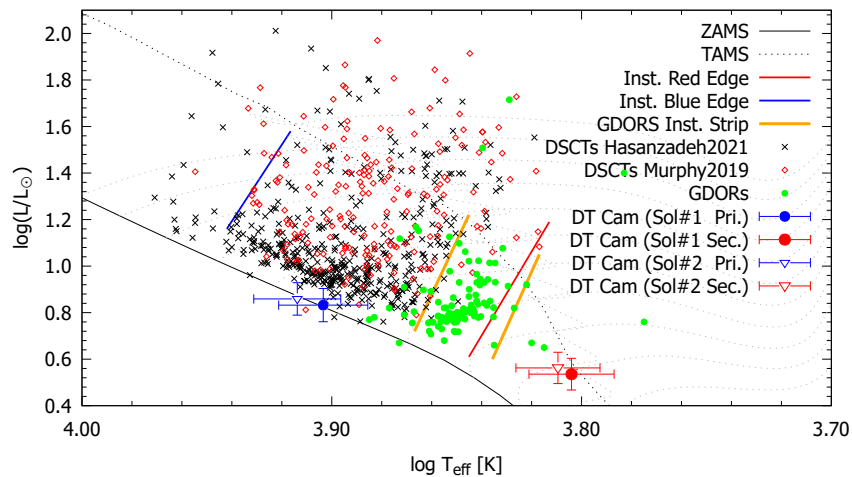
Fig. 8.   Position of the primary and secondary component of DT Cam on Hertzsprung-Russell diagram (HRD) (blue and red points, respectively). Black and gray continuous lines show ZAMS and evolutionary tracks of stars for solar metallicity composition Z=0.008 were taken from Girardi et al. (2000). Dotted red and blue lines represent the boundaries of the instability strip. Dashed orange lines indicate theoretical cool and hot boundary of γ Doradus instability strip (Warner et al. 2003). The other small dots represent the location of δ Scuti type stars obtained from Hasanzadeh et al. (2021) (black) and Murphy et al. (2019) (red). Green dots show confirmed γ Doradus stars compiled from Kaye et al. (1999), Henry et al. (2005), and Paunzen et al. (2020).

component. In the literature e.g. Sikora et al. (2019) we find some examples such as HD 13709, HD 19398, and HD 54558 which the rotational period is smaller than the obtained for the A2-type primary component in DT Cam system.

5. RESULTS AND DISCUSSIONS

We derived for the first time the absolute and geometrical parameters of the Algol type eccentric eclipsing binary DT Cam by using *TESS* and Gaia observations.The results of light-curve modelling reveal that DT Cam is a detached system with one of the components probably in the PMS phase. Using the semi-amplitudes of the radial velocity data of the system given in the catalogues, combined with our light curve solution, enabled us to find the physical and geometric parameters of the components. In this sense, we conclude that the system will make an important contribution to the literature.

We updated the light elements of the system by using all of the times of minima obtained by the *TESS* observations and data found in the literature. The difference of the orbital period obtained for primary and secondary minima is 1.079 seconds, and it is probably caused by the different time spans of the observations. In addition, we think that there is not enough time span for obtaining any apsidal motion parameters.
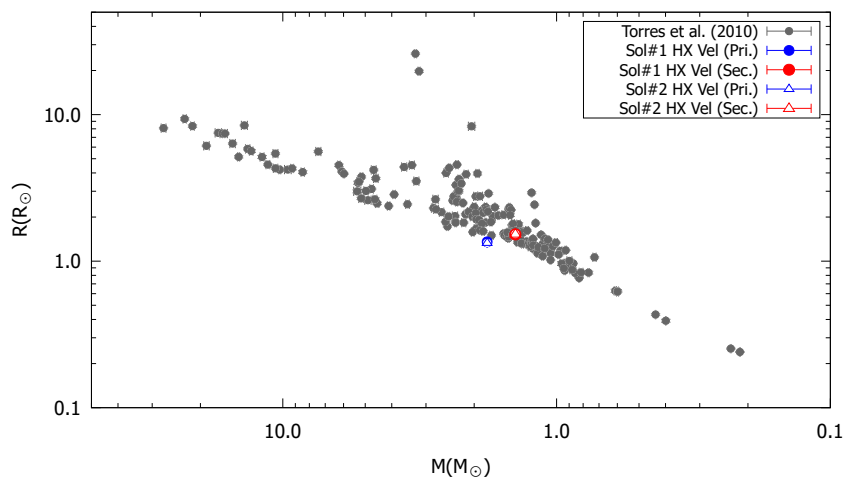
Fig. 9. Position of the primary and secondary component of DT Cam on the mass-radius diagram (blue and red points, respectively). The mass and radius values were taken from Torres et al. (2010).

In Fig.8 we plot our results with the δ Scuti type variables compiled from Uytterhoeven et al. (2011) and Murphy et al. (2019) including the γ Doradus pulsators compiled from Kaye et al. (1999), Henry et al. (2005), and Paunzen et al. (2020). The primary component located on the Main Sequence is the instability strip. Because of the location of the components on the HRD we suspected that the primary or secondary component can be a pulsator like δ Scuti, γ Doradus or rotational variable. Based on their physical and frequency analysis parameters and discussion made in the previous section we cannot strictly figure out which of the component shows small amplitude periodic variation. As a result, the secondary component can be a GDOR type pulsator or the A2-type component can be a rotating variable. Because of most of GDOR type pulsators shows multi-period variations (Zhou 2015; Paunzen et al. 2020; Takata et al. 2020; Henry et al. 2005) and we see only one for DT Cam we accepted that the primary component is a rotating variable.

The number of eclipsing binaries with a pre-main sequence component whose absolute parameters are determined is very rare. In this sense we think that the system will make an important contribution for the understanding of stellar structure and evolution.

In Fig.9 we plot our results in the mass-radius diagram given by Torres et al. (2010). The primary component seems to have small radius and low luminosity. Most likely, the primary component has a very fast rotating core, as in the EK Cep system investigated by Yıldız (2003).

As obtained in section 4 the out of eclipse variations are mostly related with the orbital frequency, except the low amplitude periodic variation with a period of 0.60597 days. It is not possible to say whether these small-amplitude periodic variations are caused by one or both components. If the periodic

variation of 0.60597 days is caused by the rotation of the primary component we can say that system is not synchronized.

6. ACKNOWLEDGMENTS

REFERENCES

Aerts, C., Christensen-Dalsgaard, J., Kurtz, D. W. 2010. Book: Asteroseismology, Published by Springer 2010 (page 680, Table 1).

Ammons, S. M., Robinson, S. E., Strader J. et al. 2006, ApJ, 638, 1004.

Avvakumova, E. A., Malkov, O. Yu. & Kniazev, A. Yu. 2013, AN, 334, 860.

Bai, Y., Liu, J. F., Bai, Z. R., Wang, S. & Fan, D. W. 2019, AJ, 158, 93.

Balona, L. A. 2011, MNRAS, 415, 1691.

Bradley, P. A., Guzik, J. A., Miles, L. F. et al. 2015, AJ, 149, 68.

Breger, M. 1990, Delta Scuti Star Newsletter, p.13-16.

Burggraaff, O., Talens, G. J. J., Spronck, J., et al. 2018, A&Ap, 617A, 32.

Cannon, A. J. & Pickering, E. C. 1993, yCat, 3135, 0.

Chandler, C. O., McDonald, I. & Kane, S. R. 2016, AJ, 151, 59C.

Eastman, J., Siverd, R. & Gaudi, B. S. 2010, PASP, 122, 935.

Eker, Z., Soydugan, F., Bilir, S. et al. 2020, MNRAS, 496, 3887.

Gaia Collaboration, 2018, 2018yCat.1345....0G.

Gaia Collaboration, 2022, 2022yCat.1355....0G.

Girardi, L., Bressan, A., Bertelli, G. & Chiosi, C. 2000, A&AS, 141, 371.

Grigahcène, A., Antoci, V., Balona, L. et al. 2010, ApJ, 713, L192.

Handler, G., Balona, L. A., Shobbrook, R. R. et al. 2002, MNRAS, 333, 262-278.

Hasanzadeh, A., Safari, H. & Ghasemi, H. 2021, MNRAS, 505, 1476.

Henry, G. W., Fekel, F. C., & Henry S. M. 2005, AJ, 129, 2815.

Henry, G. W., Fekel, F. C., & Williamson M. H. 2022, AJ, 163, 180.

Jeong, M. -J., Kim, C. -H., Song, M. -H. et al. 2020, OEJV Issue 205.

Jurysek, J., Hoňková, K., Šmelcer, L. et al. 2017, OEJV 179.

Kaye, A. B., Handler, G., Krisciunas, K. et al. 1999, PASP, 111, 840.

Kervella, P., Arenou, F., Mignard, F. & Thévenin, F. 2019, A&A, 623A, 72.

Kervella, P., Arenou, F. & Thévenin, F. 2022, A&A, 657A, 7.

Kim, C. -H., Kreiner, J. M., Zakrzewski, B. et al. 2018, ApJS, 235, 41.

Kopal, Z. 1978, ASSL (Astrophysics and Space Science Library) 68 (Dordrecht: D. Reidel Publishing Co.)

Lanza, A. F., Pagano, I., Leto, G. et al. 2009, A&A, 493, 193.

McDonald, I., Zijlstra, A. A., & Boyer M. L. 2012, MNRAS, 427, 343.

McDonald, I., Zijlstra, A. A. & Watson, R. A. 2017, MNRAS, 471, 770.

McNally, D. 1965, The Observatory, 85, 166.

Murphy, S. J., Hey, D., Van Reeth, T., & Bedding T.R. 2019, MNRAS, 485, 2380.

Otero, S. A., Wils, P. & Dubovsky, P. A. 2005, IBVS, 5586, 1.

Paegert, M., Stassun, K. G., Collins, K. A. et al. 2021, eprint arXiv:2108.04778.

Paschke, A. 2017, OEJV 181.

Paschke, A. 2019, BAV Journal No. 30.

Paschke, A. 2021, BAV Journal No. 55.

Paunzen, E., Bernhard, K., Hümmerich, S. et al. 2020, MNRAS, 499, 3976P.

Prša, A., Kochoska, A., Conroy, K. E. et al. 2022, ApJS, 258, 1.

Ricker, G. R., Winn, J. N., Vanderspek, R. et al. 2015, Transiting exoplanet survey satellite (TESS). J. Astron. Telesc. Instr. Syst. doi: 10.1117/1.JATIS.1.1.014003.

Shi, Xiang-dong, Sheng-bang, Qian, & Lin-Jia Li. 2022, ApJS, 259, 50.

Sikora, J., David-Uraz, A., Chowdhury, S. et al. 2019, MNRAS, 487, 4695.

Stassun, K. G., Oelkers, R.J., Paegert, M. et al. 2019, AJ, 158, 138.

Stellingwerf, R. F. 1979, ApJ, 227, 935-942.

Takata, M., Ouzzani, R.-M., Saio, H. et al. 2020, A&A, 635, A106.

Tonry, J. L., Denneau, L., Flewelling, H. et al. 2018, ApJ, 867, 105.

Torres, G., Andersen, J. & Giménez, A. 2010, A&ARv, 18, 67.

Uytterhoeven, K., Moya, A., Grigahcène, A. et al. 2011, A&A, A125.

Warner P. B., Kaye A. B., & Guzik, J. A. 2003, ApJ, 593, 1049.

Wilson, R. E. & Devinney, E. J. 1971, ApJ, 166, 605.

Wilson, R. E. 1979, ApJ, 234, 1054.

Wilson, R. E. 1990, ApJ, 256, 613.

Wright, C. O., Egan, M. P. & Kraemer, K. E. 2003, AJ, 125, 359.

Yıldız, M. 2003, A&A, 409, 689.

Zasche, P., Uhlar, R., Kucakova, H., Svoboda, P. & Masek, M. 2014, IBVS 6114.

Zasche, P., Uhlar, R., Svoboda, P., Kucakova, H., Masek, M. & Jurysek, J. 2017, IBVS 6204.

Zasche, P., Wolf, M., Uhlar, R., et al. 2018, A&A, 619A, 85.

Zhou, A. Y. 2015. Hybrid Pulsators - Pulsating Stars with Multiple Identities. arXiv:1501.05166.

T. Özdemir: İnonu University, Faculty of Arts and Sciences, Malatya, TURKEY. (tuncay@inonu.edu.tr)

B. Gürol: Ankara University, Science Faculty, Dept. of Astronomy and Space Sciences, 06100 Tandoğan, Ankara, TURKEY. (Birol.Gurol@ankara.edu.tr)